DARK MATTER IN SPIRAL GALAXIES. II. GALAXIES WITH HI ROTATION CURVES

STEPHEN M. KENT^{a)}

Harvard-Smithsonian Center for Astrophysics, 60 Garden Street, Cambridge, Massachusetts 02138

Received 5 November 1986

ABSTRACT

Luminosity profiles and rotation curves for 16 galaxies are analyzed to study the light and mass distribution in each galaxy. The mass distribution is modeled as the sum of bulge and disk stellar components and a dark halo. Mass/light ratios of the bulge and disk and two parameters to describe the halo are derived for each galaxy. In contrast to the situation where only optical rotation curves are available, all galaxies with H I rotation curves show evidence for dark matter. Although the relative contributions of stellar and dark matter are not well determined, the stellar component is usually close (70% or more) to its maximum possible value (the maximum-disk solution). The shapes of the luminosity profiles and rotation curves are correlated. The nature of the disk-halo conspiracy required to produce the rather featureless rotation curves is examined. It is found that the ratio of the individual peak rotation velocities from the halo and stellar components varies significantly among galaxies, showing a correlation with luminosity and/or morphological type. As an alternative to the dark matter hypothesis, Milgrom's theory of modified Newtonian dynamics is also used to analyze the rotation curves. In general, the fits to the observed rotation curves made using his gravity are satisfactory; however, two problems are that the derived value for the critical acceleration a_0 varies by a factor of 5 between galaxies, and a slightly declining rotation curve is still predicted for most galaxies but not always seen.

I. INTRODUCTION

H I rotation curves provide the best evidence for dark matter in spiral galaxies (Faber and Gallagher 1979). They usually show a constant rotation velocity extending well beyond the visible extent of a galaxy, implying that the mass distribution is much more extended than the light. One is therefore led to postulate the existence of a dark component (halo) distinct from the ordinary stellar matter. The nature of the dark matter is unknown at present.

While the existence of dark matter is thought to be well established, the relative amounts of dark and luminous matter in a galaxy are still not well known. It is not yet established whether stellar matter even dominates in the inner parts of galaxies (cf. Burstein and Rubin 1986) or if the ratio of dark to luminous matter inside some fiducial radius is constant among all galaxies. One way to overcome this problem is to combine photometric and kinematic data for a galaxy and model the observed rotation curve as the sum of contributions from luminous and dark matter. Since the distribution of dark matter is not known a priori, it is not possible to disentangle the luminous and dark components unambiguously; however, by making certain reasonable assumptions, one can still arrive at decompositions which might be sensible. From detailed decompositions one can find the stellar mass/light (M/L) ratio that is appropriate for stellar population models, measure the relative distribution of luminous and dark matter for comparison with models of galaxy formation (Blumenthal et al. 1986), and study the systematic dependence of halo properties on other properties of a galaxy. Finally, if "dark matter" actually represents a breakdown of Newtonian gravity, one can test alternative theories if they make explicit predictions.

A joint analysis of optical and kinematic data has been carried out now for a number of galaxies (Bosma and van der Kruit 1979; Kalnajs 1983; Wevers 1984; Carignan and Freeman 1985; van Albada et al. 1985). Kent (1986, hereaf-

ter referred to as Paper I) presented photometric data and analysis for 37 galaxies with optical rotation curves. This paper presents a complementary analysis of 16 galaxies with existing H I rotation curves. CCD photometry has been collected for 12 of these galaxies (data for the remaining four are taken from the literature); these observations are presented in Sec. II. Bulge/disk decompositions are discussed briefly in Sec. III. In Sec. IV, the photometry and rotation curves are analyzed to derive M/L ratios for the bulge (if present) and disk components and a characteristic radius and density for a dark halo. In contrast to the situation in Paper I, every galaxy with an H I rotation curve exhibits evidence for a dark halo. In Sec. V, these results are used to examine the questions posed above. The relationship between luminous and dark matter shows significant variation among galaxies. The relative concentration and ratio of luminous to dark matter inside some optically defined radius is correlated with galaxy luminosity and/or morphological type. Section VI presents a reanalysis of the data using Milgrom's modification of Newtonian dynamics (MOND). Rotation curves calculated using MOND provide an adequate match to observed curves, but two possible difficulties are encountered. The results are summarized in Sec. VII.

The methods of observation and analysis closely follow those of Paper I. Consequently, they will be described here only briefly.

II. OBSERVATIONAL DATA a) Sample

The complete sample of galaxies being studied is listed in Table I. Distances are usually taken from the same references as the rotation curves. For more distant galaxies, these distances are simply the Hubble distance with $H_0=75~\rm km~s^{-1}~Mpc^{-1}$. For more nearby galaxies, other distance estimators must be used. Consequently, the distances are not necessarily consistent with each other even on a relative scale.

Freeman 1985; van Albada et al. 1985). Kent (1986, here

TABLE I. Spiral galaxies with H I rotation curves.

Object	Type ^a	D (Mpc)	ε _B	ε _D	B/T	Phot.b	Rot. ^C Curve
(1)	(2)	(3)	(4)	(5)	(6)	(7)	(8)
N 224	Sb	0.67	0.30	0.70	0.19	1	1
N 247	Se	2.52	-	0.72	-	2	2
N 300	Sc	1.90	-	0.26	-	2	2
N2403	Sc	3.25	-	0.35	-	4,5	3,4
N2841	Sb	9.0	0.29	0.58	0.36	5	5
N2903	Se	6.1	-	0.52	-	5	6
N3031	Sb	3.25	0.18	0.44	0.15	5	7,8
N3109	SBm	1.7	-	0.80	-	3	9
N3198	Sc	9.2	-	0.60	-	5	10
N4236	SBd	3.25	-	0.76	-	5	3
N4258	Sb	6.6	_	0.66	-	5	11
N4736	RSab	6.0	-	0.25	-	5	12,13
N5033	Sbc	14.0	0.30	0.59	0.10	5	5,14
N5055	Sbc	8.0	0.14	0.44	0.05	5	5,14
N7331	Sb	14.0	0.60	0.60	0.26	5	4
U2259	Se	9.8	_	0.07	0.00	5	15

^aSandage and Tammann (1981)

b) Luminosity Profiles

Surface photometry has been obtained for 12 of the objects in the sample. The observations were made at the Whipple Observatory in Arizona during 1985 March to 1986 January using an RCA CCD detector. One galaxy, UGC 2259, was observed with the 61 cm telescope. The remaining galaxies have angular sizes that are too large for the field of the CCD. To overcome this problem, the CCD was equipped with a Bausch and Lomb 8000 (BL 8000) 8" (20 cm) telescope which provides a field of $16' \times 25'$ at a scale of 3'' per pixel. The CCD plus telescope assembly was attached to the side of the 61 cm telescope, which was then used for pointing and guiding. Aside from the small size of the BL 8000 telescope, the observing procedure was routine. Flat fields were obtained from images of the twilight sky. Exposures were typically 20 min. Objects were observed using the "F" and occasionally the "J" filters of Schild and Kent (1981). Magnitudes have been reduced to the r band of Thuan and

Gunn (1976). Additional details can be found in Kent (1983, 1984, 1987).

The two-dimensional frames were reduced and analyzed using standard procedures described by Kent (1983, 1984) to yield major- and minor-axis luminosity profiles. The profiles are determined by computing the average intensity along elliptical contours which are allowed to vary in position angle and ellipticity with radius. The resulting profiles are listed in Table II. Several of the profiles have been extended with either exponential laws fit to the outer parts of the profiles or by combining them with photometry from Wevers (1984).

The center of UGC 2259 has a star-like nucleus which is included in the profile. A spectrum obtained by J. Huchra with the MMT verifies that it is the galaxy nucleus.

The photometric accuracy of the profiles has been checked by Kent (1987). The east-west luminosity profile of NGC 3379 derived from a single frame agrees extremely well with the standard profile of de Vaucouleurs and Capac-

bReferences for photometry:

⁽¹⁾ Kent (1986)

⁽²⁾ Carignan (1985a)

⁽³⁾ Carignan (1985b)

⁽⁴⁾ Wevers (1984)

⁽⁵⁾ This paper

CReferences for rotation curves:

⁽¹⁾ Newton and Emerson (1977)

⁽²⁾ Carignan and Freeman (1985)

⁽³⁾ Shostak (1973)

⁽⁴⁾ Begeman (1986)

⁽⁵⁾ Bosma (1981)

⁽⁶⁾ Wevers (1984)

⁽⁷⁾ Rots (1975)

⁽⁸⁾ Visser (1980) (9) Carignan (1985b)

⁽¹⁰⁾ Van Albada <u>et al.</u> (1985) (11) Van Albada (1980)

⁽¹²⁾ Bosma, van der Hulst, and Sullivan (1977)

⁽¹³⁾ Chincarini and Walker (1967)

⁽¹⁴⁾ Van der Kruit and Bosma (1981)

⁽¹⁵⁾ Carignan, Sancisi, and van Albada (1987)

Min. Axis	19.65	20.21 20.40	20.61 20.82 21.05 21.25 21.25	21.75 21.86 21.99 22.14 22.34	22.67 23.25 23.90 24.44 24.87					6 0	19.49 19.82
Maj. Axis	19.10	19.39 19.55 19.70	19.83 19.93 20.06 20.27 20.39	20.47 20.65 20.84 21.06 21.25	21.35 21.46 21.61 21.92 22.46	22.75* 23.10*	23.48* 23.91* 24.38*	24.90* 25.47* 26.10* 26.80* 27.58*	28.43*	NGC 3198	19.49 19.58
Radius	1.05	1.29 1.43 1.58	1.75 1.94 2.14 2.37 2.62	3.20 3.54 3.91 4.32	4.78 5.28 5.84 6.46	7.99	9.76 10.79 11.93	13.18 14.57 16.11 17.80	21.74		0.00"
Min. Axis	21.23	22.17 22.43	22.68 22.97 23.34 24.03	24.87 25.32 25.88		1	15.71 15.98	16.52 17.04 17.43 17.73	18.13 18.29 18.44 18.59	18.83	19.16 19.30 19.46
Maj. Axis	19.96 19.87	19.99 20.28 20.64	20.89 21.05 21.40 21.72 22.01	22.40 22.80 23.12 23.39 23.59	23.77 24.17 24.77 25.56 25.92	NGC 3031	15.71 15.91	16.34 16.74 17.04 17.27 17.27	17.70 17.91 18.10 18.23 18.35		18.70 18.84 18.97
Radius	1.05	1.29 1.43 1.58	1.75 1.94 2.14 2.37 2.62	3.20 3.54 3.91 4.32	4.78 5.28 5.84 6.46 6.84		0.00"	5.91 8.86 11.82 14.77 17.72	20.68 23.63 26.59 29.54 33.15	37.05	45.99 51.12 56.77
Min. Axis	24.67					_	17.67 17.89	18.37 18.86 19.34 19.62 19.81	19.95 20.04 20.13 20.23 20.37	20.50	20.75 20.94 21.07
Maj. Axis	22.26	23.10 23.61 24.21	24.72* 25.35* 26.06* 26.84* 27.70*	28.65* 29.71* 30.87* 32.15*	34.52*	NGC 2903	17.67 17.72	17.95 18.28 18.67 18.99 19.15	19.24 19.31 19.39 19.48 19.63	19.75	20.04 20.05
Radius	3.20	3.54 3.91 4.32	4.78 5.28 5.84 6.46	7.89 8.72 9.63 10.65	12.45		0.00"	5.91 8.86 11.82 14.77 17.72	20.68 23.63 26.59 29.54 33.15	37.05	45.99 51.12 56.77
Min. Axis				16.71	17.78 18.40 18.87 19.26 19.58	19.85 20.07	20.24 20.39 20.57	20.67 20.76 21.02 21.23 21.47	21.77 22.06 22.33 22.68 22.94	23.23	23.78 24.02 24.29
Maj. Axis	24.29* 24.75*	24.97* 25.29* 25.90*	26.79* 27.45* 28.26* 29.11* 30.05*	NGC 2841 16.71 16.84	17.35 17.91 18.32 18.65 18.90	19.09 19.24	19.38 19.51 19.66	19.83 19.99 20.14 20.27 20.38	20.49 20.60 20.77 20.82 20.87	20.99	21.42 21.69 21.91
Radius	7.89	9.63 10.65 11.77	13.18 14.57 16.11 17.80 19.67	0.00"	5.91 8.86 11.82 14.77	20.68	26.59 29.54 33.15	37.05 41.31 45.99 51.12 56.77	1.05° 1.29 1.43 1.58	1.75	2.14 2.37 2.62
Min. Axis	_	19.49 19.47	19.50 19.62 19.72 19.80	19.97 20.07 20.13 20.20	20.46 20.57 20.67 20.81 20.96	21.13	21.32 21.30 21.32	21.45 21.77 22.14 22.61 22.94	23.18 23.44 23.60 23.96 24.34	24.56	
Maj. Axis	NCC 2403	19.49 19.49	19.51 19.56 19.62 19.70 19.78	19.84 19.89 19.95 20.01			20.70 20.77 20.84	20.89 21.03 21.30 21.55 21.55	21.86 21.99 22.08 22.23 22.54	22.87	23.40 23.59 23.88*
Radius		0.00"	5.91 8.86 11.82 14.77	20.68 23.63 26.59 29.54	37.05 41.31 45.99 51.12 56.77	1.05	1.29 1.58	1.75 1.94 2.14 2.37	2.90 3.20 3.54 3.91	4.78	5.84 6.46 7.14

-	TABLE II. (continued)	

5.91 19.74 20.54 5.91 21.73 21.71 NCC 4258 7.89 23.42 1.17 21.03 21.13 21.03 21.13 21.03 21.13 21.03 21.13 21.03 21.13 21.03 21.13 21.03 21.13 21.03 21.13 21.03 21.13 21.03 21.13 21.03 21.13 21.03 21.13 21.03 21.13 21.03 21.13 21.03	Radius	Maj. Axis	Min. Axis	Radius	Maj. Axis	Min. Axis	Radius	Maj. Axis	Min. Axis	Radius	Maj. Axis	Min. Axis	Radius	Maj. Axis	Min. Axis
20.05 20.75 11.05 21.77 21.19 21.90 10.07 17.05 17.0	5.91	19.74	20.24	5.91					8	7.89	23.42		1.75	21.03	21.51
20.55 21.10 20.66 21.69 22.30 5.91 17.41 18.10 11.93 25.03* 25.03* 25.03* 22.73 20.	11.82 14.77 17.72	20.05 20.24 20.38	20.79 20.95 21.03	11.82 14.77 17.72			0.00"	17.05 17.13	17.05 17.30	9.63 10.47 10.79	24.11 24.56 24.59*		2.14 2.37 2.62	21.31 21.55 21.91	22.09 22.48 22.95
$\begin{array}{cccccccccccccccccccccccccccccccccccc$	20.68 23.63 26.59 29.54 33.15	20.51 20.62 20.71 20.79 20.88	21.10 21.19 21.30 21.40 21.56				5.91 8.86 11.82 14.77 17.72	17.41 17.82 18.16 18.43 18.43	18.10 18.74 18.99 19.16	11.93 13.18 14.57 16.11 17.80			2.90 3.54 3.91 4.32	22.30 22.72 23.08 23.32 23.43	23.45
$ \begin{array}{cccccccccccccccccccccccccccccccccccc$	37.05 41.31 45.99 51.12 56.77	20.95 21.00 21.05 21.10 21.16	21.83 22.12 22.44 22.75 22.97				20.68 23.63 26.59 29.54 33.15		19.47 19.62 19.74 19.82	19.67 21.74	27.97* 28.75*		4.73	23.49	
$\begin{array}{cccccccccccccccccccccccccccccccccccc$	1.05	21.25	23.18	1.05			37.05	19.57	20.05		NGC 4736	·o			e
$ \begin{array}{cccccccccccccccccccccccccccccccccccc$	1.29 1.43 1.58	21.45 21.63 21.89	24.04 24.58 24.82	1.29 1.43 1.58			45.99 51.12 56.77	19.81 19.86 19.91	20.30 20.47 20.66	0.00"	15.36	15.36 15.59	0.00"	17.51 17.67	17.51 17.75
23.43 2.90 22.65 25.74 1.75 20.60 22.37 20.68 18.15 20.68 18.15 20.68 19.65 20.68 19.65 20.68 19.65 20.68 19.65 20.68 19.79 21.79 21.40 20.70 22.36 22.73 19.44 20.70 22.65 18.35 18.35 18.36 26.59 19.79 21.79 22.79 22.73 20.70 22.65 3.65 18.35 18.35 18.36 26.59 19.79 21.72 22.95 18.35 18.35 18.36 26.59 19.79 21.71 21.70 22.65 33.15 18.36 18.76 29.54 19.70 20.55 20.54 18.66 18.76 29.54 19.71 20.55 20.11 20.55 20.11 20.55 20.11 20.55 20.11 20.55 20.11 20.55 20.11 20.55 20.34 41.31 19.49 41.31 20.62 20.33 20.33 20.33 20.33 20	1.75 1.94 2.14 2.37 2.62	22.17 22.47 22.76 22.98 23.17					1.05° 1.16 1.29 1.43 1.58		20.84 21.07 21.40 21.78 22.11	5.91 8.86 11.82 14.77 17.72		16.10 16.63 17.09 17.49	5.91 8.86 11.82 14.77 17.72	18.04 18.51 18.88 19.18	18.50 19.28 19.90 20.29 20.58
78 25.41* 4.78 23.40 21.36 23.65 37.05 18.96 19.18 37.05 20.33 21.2 28 25.90* 5.28 23.69 3.20 21.56 23.94 41.31 19.11 19.49 41.31 20.62 22.25 5.84 24.11 3.54 21.88 24.28 45.99 19.81 45.99 0.62 22.2 6.46 24.43 3.51 22.47 4.55 56.77 19.82 20.09 51.12 21.03 22.03 56.77 21.19 22.11 22.24 22.47 22.47 22.43 56.77 21.19 22.19 22.24 22.33 56.77 21.19 22.19 22.19 22.23 23.33 22.13 22.13 22.13 22.13 22.13 22.13 22.13 22.13 22.11 22.19 22.19 22.13 20.53 20.73 21.19 22.19 22.24 22.13 20.53 20.73 21.66 23.96 22.	2.90 3.20 3.54 4.32	23.43 24.00 24.55 24.90*			22.65 22.73 22.79 22.89 23.03	25.74	1.75 1.94 2.14 2.37 2.62		22.37 22.60 22.82 23.09 23.35	20.68 23.63 26.59 29.54 33.15			20.68 23.63 26.59 29.54 33.15		20.86 21.21 21.46 21.65 21.65
NOC 4236 7.89 24.48 4.78 22.67 1.05′ 20.13 20.55 1.05′ 21.38 22.38 0.0" 21.73 21.74 22.22 23.16 23.16 23.16 23.42 23.24 23.24 23.16 23.16 23.42 23.24 23.24 23.16 23.16 23.42 23.24 23.24 23.16 23.16 23.42 23.	4.78	25.41 ⁴ 25.90 ⁴			23.40 23.69 24.11 24.43 24.52		2.90 3.54 3.54 4.32		23.65 23.94 24.28 24.55		18.96 19.11 19.28 19.54 19.82	19.18 19.49 19.81 20.09	37.05 41.31 45.99 51.12 56.77		21.97 22.11 22.29 22.51 22.51 22.68
9.63 25.24 5.84 22.97 1.29 20.01 20.91 1.29 21.20 22.22 23.01 1.73 21.73		NCC 423	9	7.89	24.48 24.55		4.78	22.67		1.05		20.55	1.05		
	0.00"	21.73 21.73	21.73 21.73	9.63 10.47	25.24 25.82		5.84 6.46 7.14	22.97 23.05 23.16		1.43 1.58		21.07 21.26 21.26	1.43		

(continued)	
TABLE II.	

60 24 77 24 77 24 77 24 77 24 77 25 77 25 78 26 78 26 78 26 78 26 34 34	26.05. 2. 2. 2. 2. 2. 2. 2. 2. 2. 2. 2. 2. 2.			22.11						
.49 26. .64 26. .78 26. .02 22 .22 34 .34 5055	<u> </u>	520 32 32 32 32 84 84		22.62 22.84 23.10	37.05 41.31 45.99 51.12 56.77	19.75 19.97 20.08 20.24 20.52	21.22 21.49 21.68 21.83 21.99	9.17 10.22 11.38 12.65 14.05	22.17 22.23 22.28 22.34 22.34	22.20 22.26 22.32 22.32 22.39 22.45
	4.0.0.9.	.78 28 84	22.25 22.62 22.90	23.39 23.66 23.95 24.32 24.73	1.05 1.16 1.29 1.43 1.58	20.76 20.93 21.13 21.30 21.45	22.28 22.56 22.93 23.28 23.57	15.58 17.28 19.14 21.20 23.47	22.47 22.53 22.59 22.65 22.65	22.51 22.57 22.63 22.69 22.69
NGC 5055	7.	44.	23.16 23.46 23.82 24.18 24.74	25.19	1.75 1.94 2.14 2.37 2.62	21.88 21.99 22.17 22.35 22.55	23.97 24.51 24.73 25.11 25.24	25.97 28.74 31.79 35.16 38.88	22.77 22.86 22.95 23.04 23.11	22.83 22.92 23.01 23.09 23.18
		39	25.18*			22.79	25.20	42.99		
17.18 17.18 17.33 17.42	611	7553	26.35* 27.03* 27.79*		3.54 3.91 4.32	23.53 23.77 23.85		52.55 58.09 1.07	23.54 23.83 24.15	23.73 24.05 24.42
17.76 18.00 18.33 18.50 18.60 18.83 18.77 19.00 18.92 19.14	12	.45	28.27*		4.78 5.28 5.73	24.31 25.04 26.11		1.18 1.31 1.42 1.60 1.77	24.54 25.03 25.47 26.11 26.74	24.86 25.39
.05 19 .14 19	132	NC	NGC 7331			UCC 2259		1.95	27.43	
19.22 19.75 19.29 19.92 19.35 20.08	2.0	00" 95	16.82 17.06	16.82 17.14	0.00"	20.59	20.59 20.74	2.38 2.63 2.91	29.06 30.00 31.03	
19.43 20.3 19.55 20.3 19.67 20.5 19.86 20.7 20.10 20.8	20 5.9 32 8.6 51 11.6 70 14.7	91 88 87 77	17.57 17.98 18.24 18.45 18.64	17.95 18.67 19.25 19.70 20.02	1.46 2.19 2.92 3.65 4.39	21.05 21.42 21.70 21.85 21.93	21.09 21.48 21.74 21.87 21.95	3.08	31.71	
20.27 21.02 20.39 21.18 20.49 21.35 20.62 21.55 20.76 21.82	2 20.68 8 23.63 5 26.59 5 29.54 2 33.15	нннн	8.81 8.98 9.13 9.28	20.31 20.52 20.69 20.80 20.97	5.12 5.85 6.58 7.31 8.20	21.98 22.01 22.04 22.07 22.11	22.00 22.03 22.06 22.10 22.14			

*) Profile extended by hand

cioli (1979), showing rms deviations of 0.05 mag and no systematic deviations over a span of 8 mag in surface brightness. The main source of error is uncertainty in the correction for the sky background, which is estimated to be about 1%. For most galaxies, this uncertainty translates into an error of 0.2 mag at a surface brightness $\mu_r = 24$. Three galaxies, NGC 2403, NGC 3031, and NGC 5055, still filled the field of the CCD and so their photometry is less certain at the last measured points.

All of the galaxies have some existing surface photometry, usually photographic. The largest overlap is with the work of Wevers (1984), who presents r band photometry for six galaxies in common (NGC 2403, NGC 2903, NGC 3198, NGC 4258, NGC 5033, and NGC 5055). For all but NGC 2903 and NGC 4258, the two sets of profiles agree satisfactorily: zero-point offsets range from -0.2 to 0 mag, and the rms dispersion ranges from 0.05 to 0.1 mag in the surface-brightness interval 19.5 $<\mu_r < 24.5$. These numbers are typical for comparisons between CCD and photographic data for spiral galaxies. At fainter levels, the CCD data become unreliable due to a low signal/noise ratio in the computed profiles. At bright levels, Wever's photographic plates saturate. Of the two galaxies which show worse agreement, both have pronounced spiral structure, and differences in reduction procedures are likely to contribute to the disagreement. The deviations span a range of 0.5 mag. These last two galaxies serve to emphasize the point that luminosity profiles in spiral galaxies can have uncertainties which are dominated, not by measurement error, but by nonaxisymmetric structure in the galaxies themselves.

Photometry for four remaining galaxies is taken from the literature as indicated in Table I. The luminosity profiles for all galaxies are plotted in the upper panels in Fig. 1. For reference, an exponential scale length has been estimated for all galaxies from an eyeball examination of the luminosity profiles. This scale length is given in Table III.

c) Rotation Curves

Rotation curves for all galaxies have been culled from the literature; the sources are given in Table I. All objects have H I observations, and a few have optical rotation curves. The optical rotation curves are especially valuable because the H I observations seldom have adequate resolution to map the inner portions of a galaxy. With a few exceptions, single-dish observations have not been used, since they are usually of very low resolution.

One problem with interpreting rotation curves is that it is not always clear whether they represent true circular motion in a galaxy. In three galaxies, NGC 224 (Rubin and Ford 1970), NGC 3031 (Goad 1976), and NGC 4736 (Van der Kruit 1974), optical velocities for the inner 1 or 2 kpc show evidence for noncircular motions, making it impossible to derive an accurate rotation curve in these regions. In all of these galaxies, the H I distribution has a hole in the region where the optical rotation curves are measured. The presence of noncircular motions may be correlated with the presence of a large bulge component, suggesting that the ionized gas in the center of these galaxies may not even lie in the disk. At large radii, the outer H I disk often shows warps, which further complicates the construction of the rotation curves. The rotation curve of NGC 3031 requires comment, since it is the one curve that shows a pronounced decline with radius. The observations of Rots and Shane (1975) show that the rotation curve beyond 10 kpc is not symmetrical about

the center of the galaxy, but declines steeply on one side while remaining flat on the other side. The curve adopted by Rots (1975) is an average of the two sides.

The lack of high-resolution observations of the central regions of most rotation curves means that the bulge masses will be poorly determined; in turn, the determination of other parameters is affected also.

III. BULGE/DISK DECOMPOSITIONS

Six galaxies have a significant bulge component, and for accurate mass modeling it is desirable to have a decomposition into bulge and disk components. In principle, the bulge and disk must be treated differently since they contribute in different ways to the rotation curve; also, they are likely to have different M/L ratios. In practice, the low resolution of H I rotation curves and lack of optical rotation curves for most galaxies means that little more than a bulge mass can be measured, so an accurate decomposition is not needed. Kent (1986) found traditional decomposition procedures to be unsatisfactory and developed an alternative scheme using both the major- and minor-axis profiles in which no a priori assumptions are made regarding the shapes of the bulge and disk profiles. Briefly, it is assumed that the projected bulge and disk components individually have isophotes of constant ellipticity but with a different ellipticity for each component. The galaxy major- and minor-axis profiles are each the sum of the bulge and disk profiles $\mu_{\rm B}(r)$ and $\mu_{\rm D}(r)$, but with the contributions to the minor-axis profile scaled in radius by the apparent flattenings. If the apparent ellipticities of the bulge and disk are known, then the major- and minor-axis profiles can be inverted to determine the individual bulge and disk profiles. In practice, an iterative decomposition is needed. This scheme has been used here. The decompositions are shown in the luminosity profiles in Fig. 1, and the ratio of bulge to total light is tabulated in Table I. For NGC 7331, the apparent axis ratios of the bulge and disk are similar, and so this scheme was not used; instead, a traditional decomposition into a de Vaucouleurs law bulge and exponential disk was used.

IV. MASS MODELSa) Description

The mass distribution in a galaxy is modeled as the sum of contributions from the bulge (where present), the disk, and a dark halo. The M/L ratio in the bulge and disk components individually is assumed to be constant. The bulge and halo are assumed to be spherically symmetric and the disk is assumed to be infinitely thin. While one could allow for the true flattening of the different components in the rotation-curve calculations, the computations become much more complicated without much altering the result.

The rotation curve velocity v_c is given by $v_c^2(r) = r(\partial \phi / \partial r)$, where ϕ is the gravitational potential. Expressions for $\partial \phi / \partial r$ are given in Paper I as integrals over the projected mass profile for both the bulge and disk. The halo-density profile is parametrized by the law

$$\rho = \frac{\sigma^2}{2\pi G(r^2 + a^2)},\tag{1}$$

with scale constants σ and a. This profile, while not that of an isothermal sphere, produces a flat rotation curve at large radii.

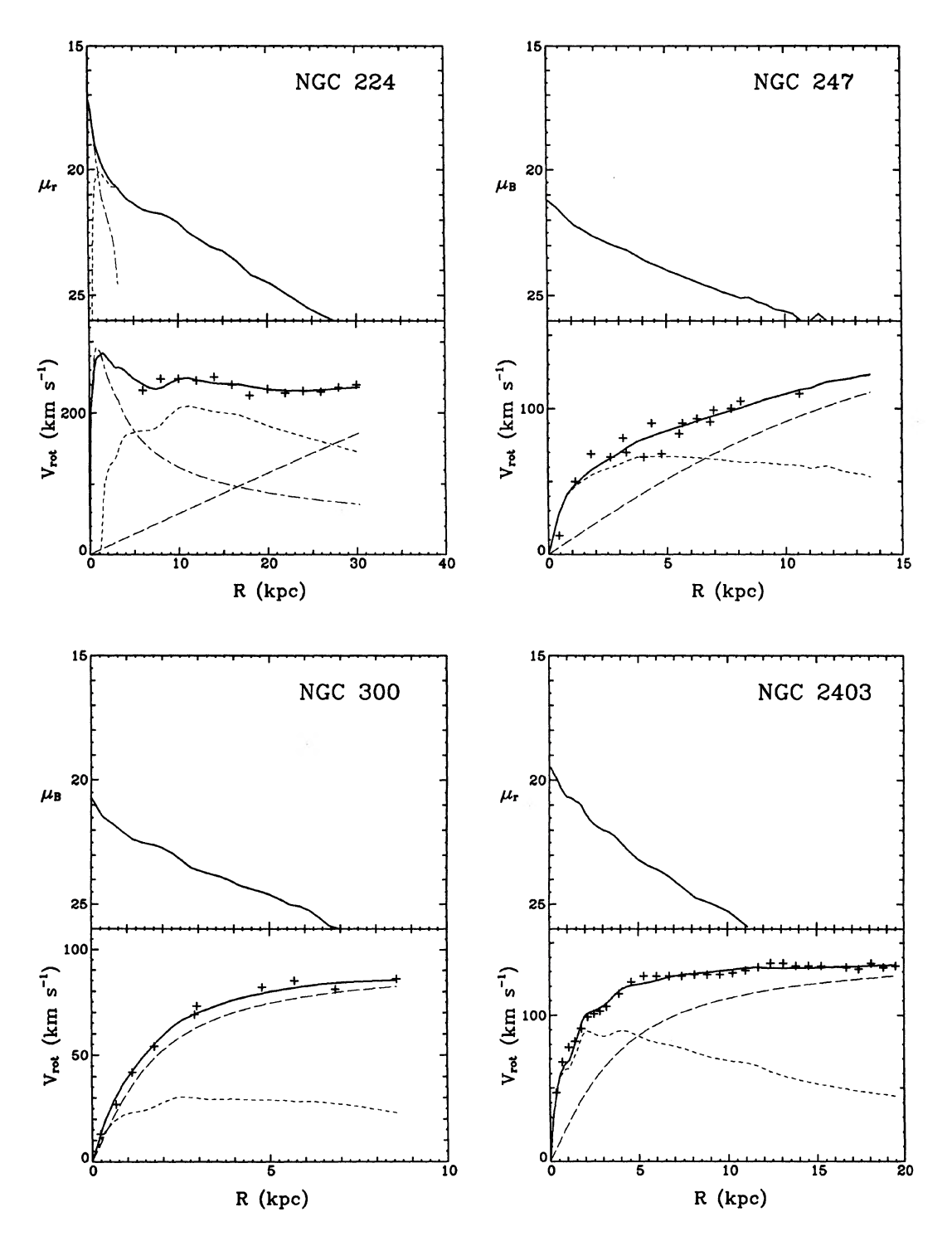
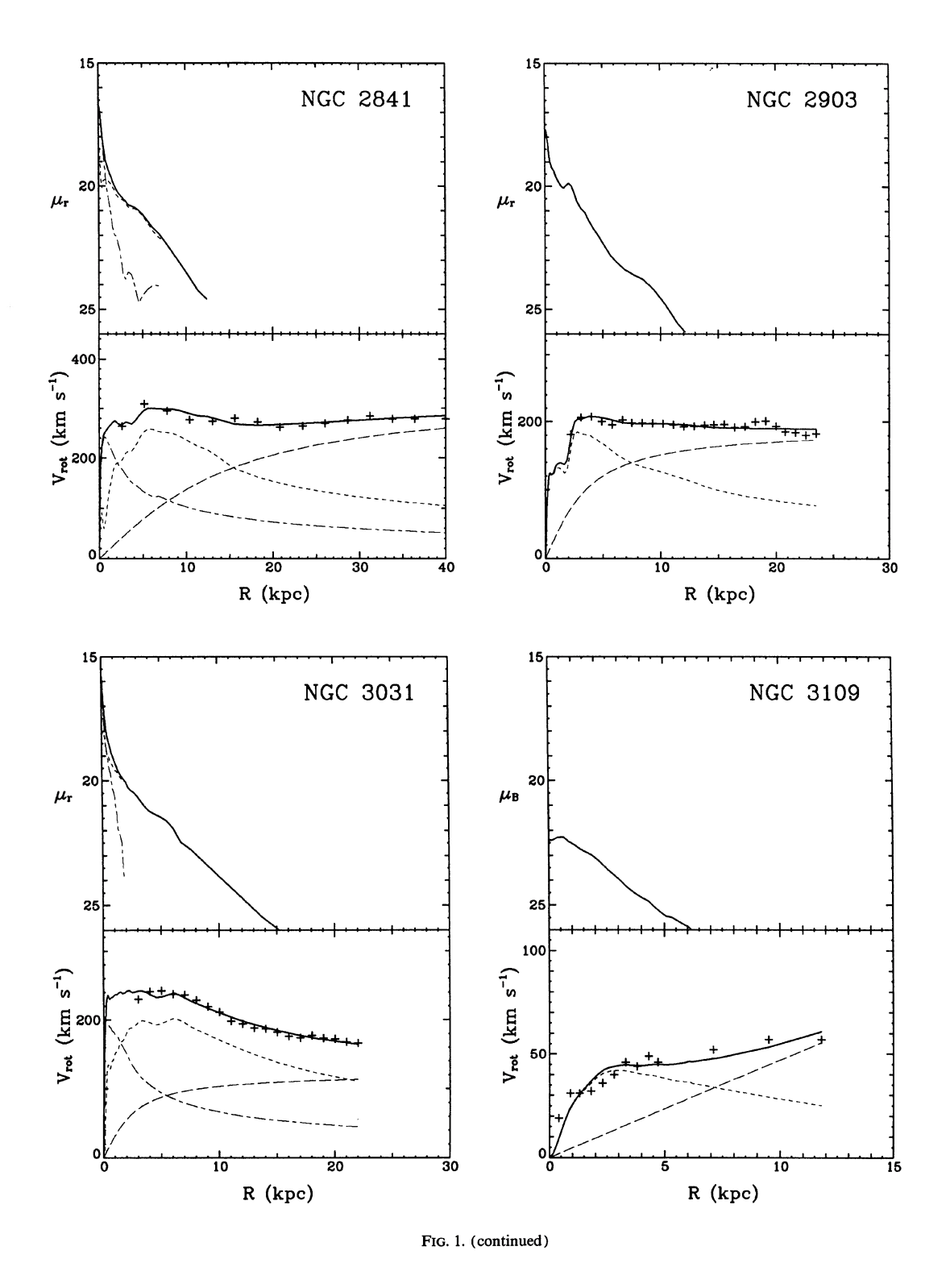
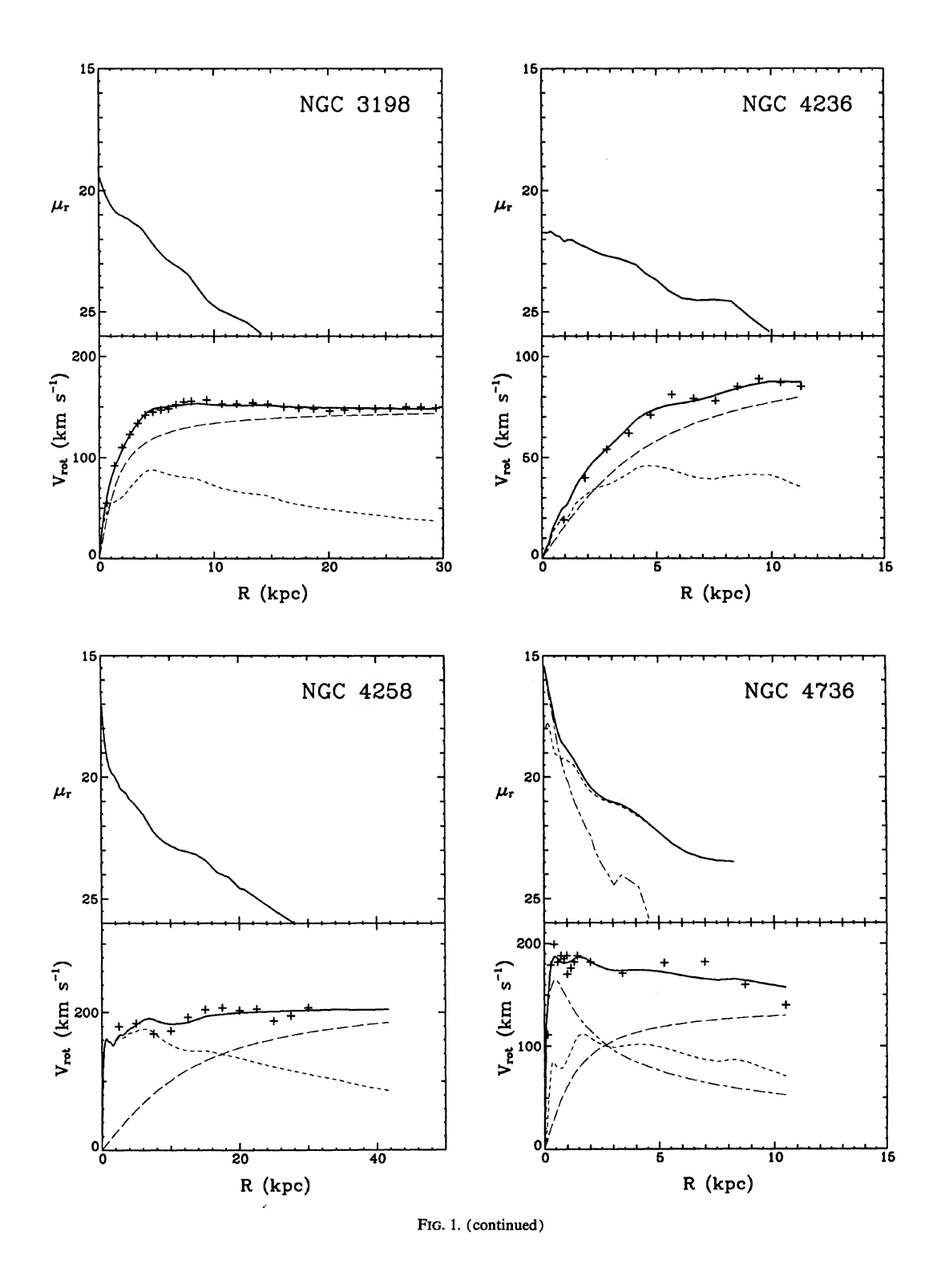


FIG. 1. Top panels: major-axis luminosity profiles for 16 spiral galaxies. The profile is decomposed into bulge (short- and long-dashed) and disk (short-dashed) components. Lower panels: observed rotation curves (pluses) and the best-fitting full solution (solid line). The separate contributions of the bulge, disk, and halo are also drawn.





© American Astronomical Society • Provided by the NASA Astrophysics Data System

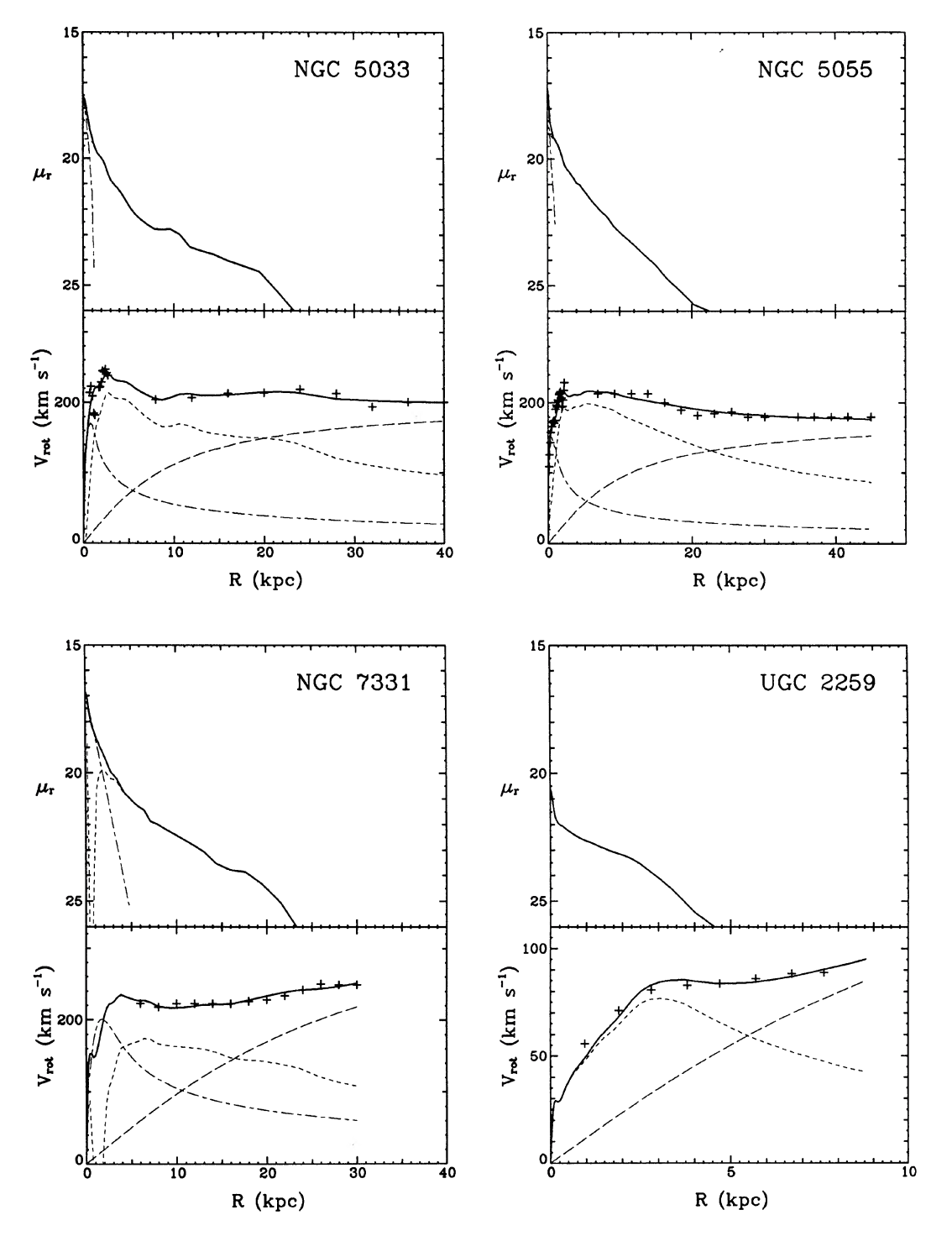


Fig. 1. (continued)

TABLE III. Scale lengths and shape parameters.

Object (1)	h (kpc) (2)	Opt. Conc. (3)	Vel. Slope (4)	Reross kpc (5)
N 224	5.24	3,85	0.00	30.
N 247	2.72	2.41	0.42	6.7
N 300	1.80	2.28	0.35	0.0
N2403	2.08	2.58	0.36	5.0
N2841	2.34	3.26	0.07	18.7
N2903	1.89	2.17	0.14	7.7
N3031	2.51	3.37	-0.03	21.
N3109	1.35	2.19	0.37	7.4
N3198	2.46	2.16	0.26	0.9
N4236	2.72	2.08	0.69	2.5
N4258	5.64	3.17	0.12	18.5
N4736	1.37:	4.29	0.02	5.6
N5033	5.96:	3.91	0.05	21.5
N5055	3.80	2.98	0.04	25.
N7331	47.4	3.44	0.15	21.5
U2259	1.34:	1.85	0.34	5.6

b) Method

The mass models have four free parameters: the bulge and disk M/L ratios, and two parameters for the halo model. These parameters are determined by making a least-squares fit to the observed rotation curve (actually to $v_{\rm c}^2$). Two solutions have been found for each galaxy. In the first, the maximum-disk solution, the halo is ignored entirely, and the bulge and disk M/L ratios are found by maximizing them consistent with fitting the rising portions of the rotation curves. This method is implemented in practice by making a normal fit to the rotation curve out to the radius where the disk contribution peaks. In the second method, a full four-parameter least-squares fit is made.

For three galaxies, NGC 224, NGC 3031, and NGC 3109, it was necessary to restrict the halo contribution. This was accomplished by keeping the halo density fixed at a constant value. For NGC 3031, it was possible to find acceptable models with any scale radius a between 0 and ∞ !

c) Results

The results from both sets of fits are listed in Tables IV and V. Most of the entries in these tables are self-explanatory. The fits from the full solution are plotted in Fig. 2. In both tables, the M/L ratios are not corrected for either internal or foreground extinction. However, in Table IV, column (5) gives the apparent luminosity while column (6) gives the luminosity corrected for foreground extinction. Extinction corrections are taken from Burstein and Heiles (1982) and are taken to be 2.5E(B-V). In column (7), $R_{\rm max}$ is the radius at which the disk rotation curve is a maximum. For the maximum-disk solution, the rms residual refers only to the portion of the rotation curve for which the fit was actually made.

For NGC 247, NGC 300, and NGC 3109, the luminosities refer to the blue bandpass. For blue spiral galaxies such as these, the luminosities (relative to solar) in the *r* bandpass should be about the same.

For NGC 3031, NGC 4736, and NGC 7331, the bulge M/L ratio in the full solution was very poorly constrained, and so it was kept fixed equal to the disk M/L ratio.

d) Shape Parameters

Since individual galaxies can have luminosity profiles and rotation curves with quite different shapes, it will be useful to provide some quantitative measure of the shapes. For luminosity profiles, a simple and straightforward measure is the luminosity concentration index of de Vaucouleurs, which is the ratio of the radii containing 75% and 25% of the total luminosity, respectively. For convenience, a parameter $c = 5 \log \left[r(75\%)/r(25\%) \right]$ will be used here. For rotation curves, no such parameter can be constructed, since the total

TABLE IV. Maximum-disk solutions.

Object	(M/L) _B	(M/L) _D	M.	\mathbf{L}_{ullet}	L*(corr)	R_{max}	rms
(1)	(2)	(3)	10 ¹⁰ M _e (4)	10 ¹⁰ L _⊕ (5)	10 ¹⁰ L _e (6)	(kpc) (7)	(8)
N 224	5.44	10.0	19.5	2.05	2.51	11.2	8
N 247	-	6.56	0.95	0.15	0.15	4.8	10
N 300	-	1.48	0.31	0.31	0.31	2.5	7
N2403	-	2.61	1.27	0.49	0.56	4.1	5
N2841	3.26	11.1	14.8	1.66	1.69	5.6	-
N2903	_	4,32	4.04	0.93	0.93	2.8	_
N3031	-0.77	5.65	8.69	1.81	1.93	6.1	6
N3109	-	3.71	0.14	0.04	0.04	3.1	6
N3198	_	5.73	2.91	0.51	0.51	4.7	10
N4236	-	6.64	0.56	0.08	0.08	4.5	6
N4258	_	4.76	8.56	1.80	1.80	6.1	3
N4736	0.74	1.47	2.48	2.09	2.09	1.7	10
N5033	4.02		9.30	1.66	1.66	2.8	17
N5055	3.79	3.38	8.49	2.50	2.50	5.5	11
N7331	5.21	3.00	11.2	2.81	3.35	6.4	-
U2259	_	6.26	0.43	0.07	0.08	3.1	_

TABLE V. Full solutions.

Object	(M/L) _B	(M/L) _D	σ	a	Po	$^{\rm M}{}_{\rm B}$	$M_{\overline{D}}$	M_{tot}	rms
			km/s	kpc	10-26	$10^{10} M_{\odot}$	10 ¹⁰ Me	10 ¹⁰ M _e	km/s
(1)	(2)	(3)	(4)	(5)	g/cm ³ (6)	(7)	(8)	(9)	(10)
N 224	7.63	8.10			12	3.6	14.8	37.4	6
N 247	-	4.66	150	11.2	45	-	0.91	4.6	8 2 3 7
N 300	-	0.42	67	1.5	499	-	0.10	1.5	2
N2403	-	1.87	103	3.3	243	-	0.90	8.2	3
N2841	5.46	8.37	232	11.6	100	2.4	9.3	74.6	7
N2903	_	3.35	135	2.9	542	-	3.2	19.4	5
N3031	3.76	3.76	86	2.0	462	1.0	6.2	13.3	5
N3109	-	7.53			10	-	0.17	1.0	5 5 2 3
N3198	_	2.05	105	1.3	1631	-	0.93	15.1	2
N4236	-	3.24	73	3.6	103	-	0.33	1.9	3
N4258	_	4.08	161	10.6	58	_	8.3	40.6	10
N4736	0.84	0.84	100	1.1	1983	0.7	1.2	5.9	11
N5033	4.08	5.59	143	7.5	91	0.7	8.6	37.1	13
N5055	3.79	3.33	125	8.2	58	0.4	7.8	32.7	9
N7331	4.04	4.04	308	27.2	32	4.8	7.3	43.3	3
U2259	_	5.35	133	9.1	53	_	0.4	1.8	3

mass does not converge in the domain of the rotation curves. Instead, the average logarithmic slope $\langle d(\ln v)/d(\ln r)\rangle$ has been computed. For convenience, the slopes were computed from the best-fitting model at the same radii for which the luminosity profiles were tabulated. Although the mean slope so computed depends on the range in radius covered by the rotation curve, it still provides a useful means of characterizing slowly rising versus flat rotation curves. The concentration and slope parameters are listed in Table III.

V. DISCUSSION

a) Comparison of Maximum-Disk and Full Solutions

In no case does the maximum-disk solution produce a good fit to the entire rotation curve: a halo component is

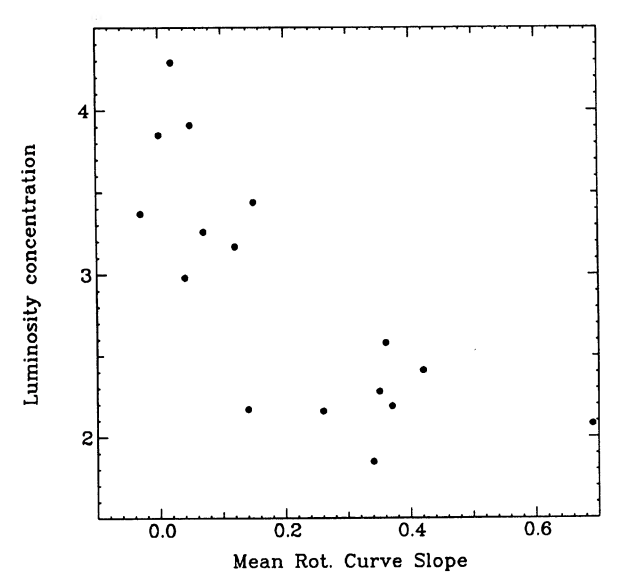


FIG. 2. Correlation between luminosity concentration and mean slope of the rotation curve.

always required. The one possible exception is NGC 3031, which has a declining rotation curve. This need for a dark halo contrasts with the case where optical rotation curves alone are used: in Paper I the evidence for dark halos was found to be much weaker. The reason for the contrast is that H I rotation curves extend much farther in radius relative to optical curves and are able to sample radii where the halo mass dominates.

Unfortunately, even with the leverage provided by extended H I rotation curves, the various parameters are still tightly coupled in the least-squares solution. The correlation coefficients between the various parameters often exceed 90%. Consequently, the results of the fits must be used cautiously. Van Albada et al. (1984) have also emphasized the ambiguity in separating the stellar and halo components in NGC 3198. The reason is that the chosen parametric form for the halo-density law produces a rotation curve that by itself makes a reasonable fit to the observed rotation curves. Since the true density law for the halo is not known, little can be done to alleviate this difficulty.

Even so, in 12 out of 16 objects, the stellar mass from the full solution is 72% or more of that from the maximum-disk solution. This result is about what would be expected if one took the maximum-disk solution and lowered the M/L ratios until one obtained a reasonable halo-density profile which declined monotonically from the center. E. G. van Albada et al. (1985) found that for NGC 3198 a disk M/L ratio 87% of its maximum-disk value produces a physically plausible halo. For the remaining four objects, the stellar mass from the full solution is substantially lower; however, because the least-squares solutions are so degenerate, one could force the M/L ratios close to their maximum-disk values and still find an acceptable solution.

b) Distribution of Parameters

In Paper I it was found that the apparent M/L ratio of the stellar component correlated with inclination, morphological type, and luminosity. The present sample of galaxies is

too small and heterogeneous to verify these trends. The maximum-disk M/L ratios scatter primarily between 3 and 10 (corrections for internal extinction would reduce these somewhat). This range is very similar to that found in Paper I (after allowing for differences in Hubble constant). The median M/L ratio from the full solution is about 4.5. If the corrections for internal extinction from Paper I are applied, the true M/L ratio is about 2.5. This value is almost identical to that found in Paper I for an Sbc galaxy (again after allowing for differences in Hubble constant).

Of the halo parameters, the velocity dispersion is the best determined, especially for galaxies where the rotation curve extends well into the halo-dominated region. The core radius is rather tightly coupled to the disk and bulge M/L ratios and so is less well determined, as is the central density. The smallest core radius in Table V is 1.1 kpc for NGC 4736; the largest that can be measured is 27 kpc for NGC 7331. The lowest central densities are found for those objects where the halo was fixed at a constant density throughout, reaching as low as 10 (in units of 10^{-26} g cm⁻³). The highest is about 2000 for NGC 4736.

To see if the large range in halo radii and densities is real or if it is a result of the tight coupling of parameters in the least-squares fit, a second set of solutions was made keeping the bulge and disk M/L ratios fixed at their maximum-disk values. The derived parameters changed somewhat, but not nearly enough to reduce the observed range: the maximum core radius and minimum density varied only slightly. The smallest core radius (2.8) kpc and highest density (294) were still found for NGC 4736. Median halo parameters are about a=8 kpc, $\rho_0=6.3\times10^{-25}$ g cm⁻³, and $\sigma=130$ km s⁻¹. In Paper I a loose trend between ρ_0 and mass was found; however, that trend is not seen here.

Another way to assess the contribution of the halo to a galaxy is by measuring the radius where the halo mass equals the stellar mass relative to some fiducial radius such as the exponential scale length of the disk. Crossover radii $r_{\rm cross}$ are tabulated in Table III. The ratio $r_{\rm cross}/h$ ranges from less than 1 in NGC 4236 to more than 8 for NGC 3031. There is somewhat of a trend for galaxies of low luminosity to be relatively more dominated by dark matter (i.e., low $r_{\rm cross}/h$) compared with high-luminosity galaxies.

c) Profile Shapes

If the stellar M/L ratios are close to their maximum-disk values, then for nearly all objects the stellar mass dominates the inner parts of a galaxy. In such a case one would expect a correlation between the shape of the inner rotation curve and the shape of the luminosity profile. Even though many of the rotation curves here have limited resolution in the center, a casual examination of the objects in Fig. 1 shows a good correspondence between the shapes of the luminosity profiles and rotation curves. Systems with low luminosity concentration (no central bulge) such as NGC 247, NGC 300, NGC 4236, and UGC 2259 have slowly rising rotation curves, and in some cases it is not clear that the peak in the curve has even been reached. In contrast, systems with high luminosity concentration such as NGC 2841, NGC 4736, NGC 5033, and NGC 5055 have rotation curves that rise much more rapidly and are then flat or even slightly declining over most of their observed range. These trends can be made more quantitative: Fig. 2 shows the relation between the optical concentration and the mean slope of the rotation curve from Table III. A clear relation is seen. Furthermore,

both the optical concentration and rotation-curve shape are correlated with the luminosity of a galaxy: in Fig. 2, the galaxy luminosity tends to increase in going from the upper left to lower right. A relation between rotation-curve shape and luminosity has been found previously by Rubin *et al.* (1982, 1985) and Burstein *et al.* (1982).

Further evidence that the stellar mass dominates in the inner parts of a galaxy could come from matching features in the rotation curves with corresponding features in the luminosity profiles. Again, the low resolution of H I observations makes this difficult. Also, perturbations to pure circular motion can complicate any detailed interpretation of rotation curves' behavior. In NGC 2403, however, where the H I observations are exceptionally good, there is a match between breaks in the rotation curve at 2 and 4 kpc with steps in the luminosity profile at the same radii. In NGC 3198, there is somewhat weaker evidence for the same kind of behavior.

d) Disk-Halo Conspiracy

A notable property of rotation curves is that they are remarkably flat and featureless. If stellar matter dominates in the inner part of a galaxy and dark matter outside, then the peak rotation velocity due to the stellar component must be about the same as that due to the halo in order that they combine to produce the observed flat profile. This apparent coincidence is referred to as the disk-halo conspiracy.

In current theories of galaxy formation which allow for both a luminous and dark component, the difference in distribution between stellar (baryonic) matter and dark matter is explained by the fact that the stellar matter can dissipate energy during the collapse and formation of a galaxy while the dark matter (if it is composed of noninteracting particles) cannot. The final distribution of the two components depends upon their initial distribution and the degree of dissipation which in turn depends on the initial specific angular momentum acquired by the protogalaxy (Faber 1982; Blumenthal et al. 1984) The shape of the resulting rotation curve can be rising, flat, or falling, depending on these various factors (Blumenthal et al. 1986). If there is a conspiracy between the disk and halo components, then this galaxy-formation picture is constrained in a way which is not understood

An inspection of the various rotation-curve fits in Fig. 1 shows that the individual components display a considerable variety of shapes and that there is no single relation between the disk and halo contributions. One way of characterizing the conspiracy is by comparing the peak velocity from the maximum-disk solution with the asymptotic (or last measured) rotation velocity. In most low-luminosity objects, the peak disk velocity falls short of the asymptotic velocity, missing by 30% in extreme cases. Since the true disk M/Lratio is likely to be lower than its maximum-disk value, this shortfall is likely to be even larger. Other galaxies show the opposite behavior: in NGC 4736 the peak bulge-plus-disk velocity (from either solution) is larger than the asymptotic halo velocity by 30% or more. Hence the ratio between the peak disk velocity and halo velocity is not universal. However, there is a reasonably good correlation of this ratio with galaxy luminosity (NGC 4736 is unusual in that it has a high luminosity but otherwise has a small mass and size).

Since the relative concentration of luminous to dark matter in a galaxy is related to the amount of dissipation that occurred during the collapse phase, more highly concentrated galaxies should have a higher characteristic surface

brightness, a more steeply rising rotation curve, and a higher ratio of stellar to dark matter inside some characteristic optical radius compared with low-concentration galaxies. All of these features are found in the present set of galaxies. Furthermore, Faber (1982) and Blumenthal *et al.* suggest that the degree of dissipation is also related to the morphological type of a galaxy. In fact, that trend is also seen here, since the high-concentration, high-luminosity galaxies are of type Sab—Sbc while the lower luminosity systems are all of type Sc or later. However, the sample is too small to say whether the correlation is primarily with type, luminosity, or both.

e) Constraints on Dark Matter Particle Mass

Tremaine and Gunn (1979) have shown that one can use measurements of the central halo density and velocity dispersion to place constraints on the mass of neutrinos or any other weakly interacting particles that might compose the dark matter, provided such particles were still relativistic when they decoupled from the universe after the big bang (so-called hot dark matter). The essence of their argument is that the phase-space density of dark matter $f \approx \rho_0/\sigma^3$ cannot exceed a maximum value which is of order $2h^{-3}$ (h being the Planck constant). They show that as a consequence the mass of a neutrino must satisfy

$$m > 9.8 \left(\frac{100 \text{ km s}^{-1}}{\sigma}\right)^{3/4} \left(\frac{\rho_0}{10^{-26} \text{ g cm}^{-3}}\right)^{1/4} \text{g}^{-1/4} \text{ eV},$$
(2

where $1 \le g \le 2$ is the neutrino helicity. Tremaine and Gunn use values for ρ_0 and σ that are essentially the same as the median values given above and derive a lower limit on the neutrino mass of order 20 eV. However, a flaw in this reasoning is that one should use the central velocity dispersion of the halo in Eq. (2), not its asymptotic value. If the dark matter is sitting in hydrostatic equilibrium in the potential well of a galaxy, then the local velocity dispersion of the dark matter is not constant but varies significantly with radius. The central dispersion can be 2 or 3 times the asymptotic value. Hence the lower limit on m should be quite a bit lower (of order 10 eV). In fact, since the true central density and velocity dispersion are actually quite poorly known, this test does not yet provide a stringent lower limit on the neutrino mass. Malagoli and Ruffini (1986) also have explored this problem by considering several possible halo configurations and arrived at the same conclusion.

f) On the Ubiquity of Halos

The apparent need for a halo component in every galaxy in this sample is obviously consistent with the notion that all galaxies have dark halos. However, in Paper I it was found that about 1/3 of all galaxies do *not* require halos to explain their rotation curves. How can one resolve the apparent discrepancy between these two results?

One obvious explanation already mentioned is that the optical rotation curves used in Paper I do not extend far enough in radius to show the existence of a halo, and if one could obtain extended H I data, presumably they would all show flat rotation curves as well. Some support for this idea comes from noting that the rotation curves in Paper I reach only to a surface brightness of typically $\mu_r = 23-24$ mag arcsec⁻². If one took the H I rotation curves used in this paper and truncated them at a similar radius, then the evidence for halos would be much less convincing and in some cases one might very well conclude that no halo is needed.

However, there is also the possibility of a selection bias if somehow the existence of dark halos and extended H I envelopes are related. Some weak evidence that this might be the case comes from the work of Bosma (1981b), who finds that the ratio of hydrogen surface density to the equivalent halo mass density is approximately constant in a galaxy beyond the edge of the optical disk. If the existence of extended H I disks requires the presence of dark halos, then clearly galaxies with rotation curves measured by H I observations will always show dark halos, while galaxies selected for optical rotation curves may not.

VI. ALTERNATIVES TO DARK MATTER

The existence of dark matter in galaxies seems unavoidable in the context of conventional Newtonian gravity but is aesthetically unpleasing. Milgrom (1983a,b) has suggested that instead the laws of gravity need modification in the regime of small accelerations. In the original formulation of modified Newtonian dynamics (MOND), he proposes a new equation for computing the gravitational acceleration of a particle:

$$\mu(x)g = g_{N}. \tag{3}$$

Here, g_N is the conventional Newtonian acceleration computed in the standard way, g is the true acceleration, x = g/ a_0 , where a_0 is a constant, and $\mu(x)$ is a function with the property that $\mu \approx 1$ for $x \gg 1$ and $\mu \approx x$ for $x \ll 1$. The function μ and the constant a_0 are not specified a priori and must be determined from observation. The rotation curve of a galaxy is given by $v_c^2 = rg(r) = rg_N(r)/\mu(x)$. In the regime $x \ge 1$, ordinary Newtonian dynamics are recovered. For $x \le 1$, one has $g \approx (g_N a_0)^{1/2} = (GMa_0)^{1/2}/r$ and the asymptotic rotation velocity is given by $v_\infty^2 = rg = (GMa_0)^{1/2} = \text{constant}$. Here, M is the total mass inside a given radius. Beckenstein and Milgrom (1984) have derived a Lagrangian formulation for MOND which results in a more complicated procedure for computing accelerations in most cases. However, Milgrom (1986) shows that Eq. (3) still works well for computing rotation curves for most expected mass distributions, so this equation will still be retained. Milgrom has proposed various forms for the function $\mu(x)$. Here, the function $\mu(x) = x/(1+x^2)^{1/2}$ will be used, since it works somewhat better than others.

A few interesting properties result from using MOND to compute rotation curves. For galaxies with a high mass density, the computed rotation curve will be the normal Newtonian curve out to some transition radius $r_{\rm t}$ where $v^2/r \approx a_{\rm 0}$. The shape of the curve is determined by the shape of the mass distribution, and the amplitude by the M/L ratio. At the opposite extreme, for a galaxy with a low mass density, the rotation curve has a different shape, but again determined only by the shape of the mass distribution. If $v_{\rm N}(r)$ is the former and $v_{\rm M}(r)$ the latter curve, then to within a constant they are related by $v_{\rm M} \propto (v_{\rm N}^2 r)^{1/4}$. An intermediate-density galaxy will have a rotation curve given by $v_{\rm N}$ inside $r_{\rm t}$ and $v_{\rm M}$ outside, patched together at $r_{\rm t}$ in a manner that depends on the exact form of $\mu(x)$.

In the high mass density limit, the rotation curve is insensitive to a_0 and is proportional to the M/L ratio. In the low density limit, the rotation curve is sensitive to the product $(M/L)a_0$ but neither parameter separately. Consequently, to determine the parameter a_0 , galaxies of intermediate mass density are needed.

A curious feature of MOND for disk galaxies is that although the dynamical laws were invented to produce flat rotation curves at large radii, the rotation curves computed in this theory still decline slightly. This can be seen by considering the rotation curve of an exponential disk for which Freeman (1970) has computed the ordinary rotation curve $v_N(r)$. The quantity $v_N^2 r/G$, which equals the disk mass M as $r \rightarrow \infty$, actually exceeds M for radii greater than about 2.8 scale lengths, reaching a maximum of 1.21M at about 4 scale lengths. Consequently, in the low density limit, the MOND rotation curve will have a peak value of $1.05v_{\infty}$ at this radius. In objects of intermediate density or galaxies with spheroidal components, the peak usually will be higher still. This feature is independent of the shape of the function $\mu(x)$ and is simply a consequence of rotation curves produced by disk mass distributions. More detailed calculations by Milgrom (1986) using the exact theory also show the same effect.

MOND has been used to computed rotation curves for the 16 galaxies with stellar M/L ratios and a_0 taken as free parameters. Since the value of a_0 so derived is inversely proportional to the distance assigned to a galaxy, and the relative distance scale used here is probably not uniform, some scatter is expected in the deduced values of a_0 . Milgrom (1983b) suggests a rough value for a_0 of about 2.7×10^{-8} cm s⁻² (for $H_0 = 75$).

Of the 16 galaxies studied here, only seven yield a useful estimate of a_0 . These values are listed in Table VI. The transition radius r_t always lies within the range of the measured rotation curve. For five other galaxies, the entire rotation curve falls in the low-density regime. In the remaining four galaxies, the inner rotation curve is not measured well enough; otherwise they too could yield a useful value for a_0 . Typical fits to the rotation curves of six galaxies are shown in Fig. 3. For galaxies in the low-density limit, a value for a_0 of 1×10^{-8} is used. NGC 2403 is also best fit by a model in the low-density limit but requires a value for $a_0 > 3 \times 10^{-8}$.

The seven values of a_0 from Table VI span a factor of 5

TABLE VI. MOND solutions.

0bject	(M/L) _B	(M/L) _D	a _o	rms	r_{t}
			10-8	km/s	kpe
			cm/s2		
(1)	(2)	(3)	(4)	(5)	(6)
N 224	8,22	7.18	1*	8	17
N 247	-	3.68	1*	9	<
N 300	-	1.23	1*	7	<
N2403	_	1.28	>3	4	<
N2841	6.63	6.57	3.3	10	6.9
N2903	_	5.50	1*	19	9.4
N3031	4.41	4.41	0.60	6	15
N3109	-	1.10	1*	6	<
N3198	-	3.95	1.65	4	0.1
N4236	-	3.23	1*	6	<
N4258	_	3.84	1.48	11	3.0
N4736	0.70	1.56	1.46	10	5.6
N5033	4.04	5.70	1.23	14	9.6
N5055	3.73	3.41	0.84	9	14
N7331	4.86	4.86	1*	19	14
U2259	_	4.22	1*	4	<

^{*)} Value fixed

with a median of about 1.2×10^{-8} . Even allowing for uncertainties in determining individual values, this range is uncomfortably large. The extreme values come from NGC 3031 and NGC 2841. In both cases, using a fixed value of 1×10^{-8} produces markedly inferior fits.

Overall, the fits with MOND are good, although not quite as good as with the dark halo models. This, in itself, is not surprising since the MOND model has one less free parameter, which should be identical for all galaxies. One success of MOND is that it accounts reasonably well for the mass discrepancies in both the high- and low-luminosity galaxies, which have much different rotation-curves shapes. One potential problem for MOND is in reproducing the slope of the outer rotation curve. As noted above, MOND predicts a very slightly falling rotation curve at large radii in the lowdensity limit; in higher-density galaxies the drop should be larger. In a few galaxies, most notably NGC 5055, such a decline is seen. In other cases, however, the observed curve is flat or still rising at the last radius, the most notable cases being UGC 2259 and NGC 7331. Even so, this discrepancy is not necessarily significant. One can argue that the observed rotation curves are slightly in error, since the H I distribution is often warped in the region where the declining rotation curve is expected. A second possibility is that there is additional light and hence mass at large radii which is just too faint for current photometry to pick up. Finally, it is possible that a modest variation in the stellar M/L ratio could also alleviate the apparent discrepancy.

Sanders (1986) has discussed a few other problems for MOND. He points out that the observed mass in H I in NGC 3109 exceeds by a factor of 2 the total dynamical mass calculated from MOND. A similar problem is encountered in comparing gas and dynamical masses in some x-ray clusters of galaxies.

Because of problems in accurately measuring rotation curves, determining distances to galaxies, and converting photometry to stellar mass profiles, rotation curves by themselves do not yet provide convincing support or disproof of the validity of MOND. More critical tests of MOND may be encountered in other settings.

VII. CONCLUSIONS

Extended H I rotation curves leave little doubt as to the existence of unseen matter in galaxies. Photometry and rotation curves for 16 galaxies have been used to construct mass models consisting of a bulge, disk, and a dark halo. M/L ratios for the bulge and disk components and two scale parameters for the halo have been derived from a least-squares fit of the model to the observed rotation curves.

Although the parameters are tightly coupled in the least-squares solution, the bulge and disk M/L ratios usually come close to (more than 70% of) their maximum possible values. They still cover a broad range from less than 1 to greater than 8 in solar units (uncorrected for extinction and using $H_0 = 75$). The median extinction-corrected value is about 2.5. Typical halo parameters are $\sigma = 130$ km s⁻¹, a = 8 kpc, and $\rho_0 = 6.3 \times 10^{-25}$ g cm⁻³.

Although the sample of galaxies is small, there is a well-defined trend in photometric and rotation-curve properties with luminosity and mass: as the luminosity of a galaxy increases, it has increased surface brightness, a more concentrated luminosity profile, a more steeply rising rotation curve, and a lessened domination by dark matter. These

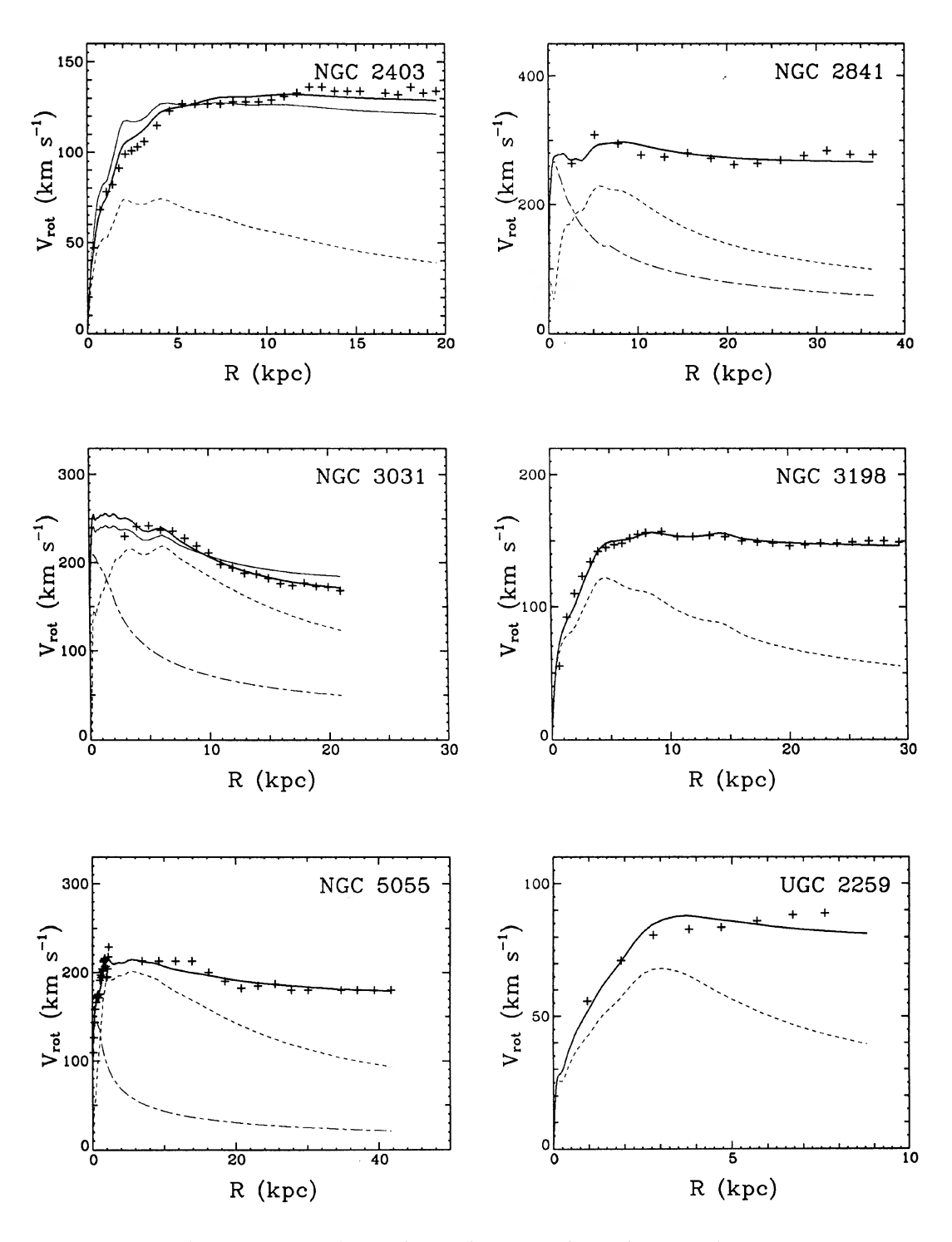


Fig. 3. Examples of six rotation curves with best-fitting model computed using Modified Newtonian Dynamics (MOND). The characteristic acceleration a_0 has been adjusted to give the best fit for each galaxy. For NGC 2403 and NGC 3031, the narrow solid lines show the result of fixing a_0 at a value of 1×10^{-8} g cm⁻³.

trends are consistent with a picture of galaxy formation in which baryonic matter within a dark matter halo dissipates energy during the collapse phase; the trends just discussed imply that more luminous galaxies undergo a greater degree of dissipation.

As an alternative to the dark matter hypothesis, Milgrom's modification to gravity, MOND, has been used as well in modeling the rotation curves. MOND works nearly as well as dark matter models in fitting the observed rotation curves with one less degree of freedom. However, the scale parameter a_0 shows an uncomfortably large variation among galaxies; also, MOND predicts that all rotation curves

should show a very slight decline with radius, which seems to be violated in some objects.

I am indebted to George Atamian and the Bushnell Division of the Bausch and Lomb Corporation for generously donating the BL 8000 telescope used for these observations. I wish to thank Mike Frankston for assisting with the observations, Renzo Sancisi for providing the rotation curves of NGC 2403 and UGC 2259 in advance of publication, and J. Huchra for obtaining the spectrum of the UGC 2259 nucleus. This work was partially supported by NSF grant AST-84-51724.

REFERENCES

Beckenstein, J., and Milgrom, M. (1984). Astrophys. J. 286, 7.

Begeman, K. (1986). Preprint.

Blumenthal, G. R., Faber, S. M., Flores, R., and Primack, J. R. (1986). Astrophys. J. 301, 27.

Blumenthal, G. R., Faber, S. M., Primack, J. R., and Rees, M. J. (1984). Nature 311, 517.

Bosma, A. (1981a). Astron. J. 86, 1791.

Bosma, A. (1981b). Astron. J. 86, 1825.

Bosma, A., van der Hulst, J. M., and Sullivan, W. T. (1977). Astron. Astrophys. 57, 373.

Bosma, A., and van der Kruit, P. C. (1979). Astron. Astrophys. 79, 281.

Burstein, D., and Heiles, C. (1982). Astron. J. 87, 1165.

Burstein, D., and Rubin, V. C. (1985). Astrophys. J. 297, 423.

Burstein, D., Rubin, V. C., Thonnard, N., and Ford, W. K. (1982). Astrophys. J. 253, 70.

Carignan, C. (1985a). Astrophys. J. Suppl. 58, 107.

Carignan, C. (1985b). Astrophys. J. 299, 59.

Carignan, C., and Freeman, K. C. (1985). Astrophys. J. 294, 494.

Carignan, C., Sancisi, R., and van Albada, T. S. (1987). Preprint.

Chincarini, G., and Walker, M. F. (1967). Astrophys. J. 147, 407.

de Vaucouleurs, G., and Capaccioli, M. (1979). Astrophys. J. Suppl. 40, 699.

Faber, S. M. (1982). Astrophysical Cosmology, edited by H. A. Bruck, G. V. Coyne, and M. S. Longair (Pontifica Academia Scientarum, Vatican City), p. 191.

Faber, S. M., and Gallagher, J. S. (1979). Annu. Rev. Astron. Astrophys. 17, 135.

Freeman, K. C. (1970). Astrophys. J. 160, 811.

Goad, J. W. (1976). Astrophys. J. Suppl. 32, 89.

Kalnajs, A. (1983). In Internal Kinematics and Dynamics of Disk Galaxies, IAU Symposium No. 100, edited by E. Athanassoula (Reidel, Dordrecht), p. 87.

Kent, S. M. (1983). Astrophys. J. 266, 562.

Kent, S. M. (1984). Astrophys. J. Suppl. 56, 105.

Kent, S. M. (1986). Astron. J. 91, 1301 (Paper I).

Kent, S. M. (1987). Astron. J. (in press).

Malagoli, A., and Ruffini, R. (1986). Astron. Astrophys. 157, 293.

Milgrom, M. (1983a). Astrophys. J. 270, 365.

Milgrom, M. (1983b). Astrophys. J. 270, 371.

Milgrom, M. (1986). Astrophys. J. 302, 617.

Newton, K., and Emerson, D. T. (1977). Mon. Not. R. Astron. Soc. 181, 573.

Rots, A. (1975). Astron. Astrophys. 45, 43.

Rots, A., and Shane, W. W. (1975). Astron. Astrophys. 45, 25.

Rubin, V. C., Burstein, D., Ford, W. K., and Thonnard, N. (1985). Astrophys. J. 289, 81.

Rubin, V. C., and Ford, W. K. (1970). Astrophys. J. 159, 379.

Rubin, V. C., Ford, W. K., Thonnard, N., and Burstein, D. (1982). Astrophys. J. 261, 439.

Sancisi, R., and van Albada, T. S. (1985). In Dark Matter in the Universe, IAU Symposium No. 117, edited by J. Kormendy and J. Knapp (Reidel, Dordrecht).

Sanders, R. H. (1986). Mon. Not. R. Astron. Soc. 223, 539.

Schild, R., and Kent, S. (1981). Proc. SPIE 290, 186.

Shostak, G. S. (1973). Astron. Astrophys. 86, 1791.

Thuan, T. X., and Gunn, J. E. (1976). Publ. Astron. Soc. Pac. 88, 543.

Tremaine, S., and Gunn, J. E. (1979). Phys. Rev. Lett. 42, 407.

van Albada, T. S. (1980). Astron. Astrophys. 90, 123.

van Albada, T. S., Bahcall, J. N., Begeman, K., and Sancisi, R. (1985). Astrophys. J. 295, 305.

van der Kruit, P. C. (1974). Astrophys. J. 188, 3.

van der Kruit, P. C., and Bosma, A. (1981). Astron. Astrophys. Suppl. 34, 259.

Visser, H. C. D. (1980). Astron. Astrophys. 88, 149.

Wevers, B. M. H. (1984). Ph. D. thesis, Groningen University.